

Electrons trapped in magnetic controlled gapped graphene-based quantum dots

Mohammed El Azar,¹ Ahmed Bouhlal,¹ and Ahmed Jellal^{1,2}

¹*Laboratory of Theoretical Physics, Faculty of Sciences,
Chouaib Doukkali University, PO Box 20, 24000 El Jadida, Morocco*

²*Canadian Quantum Research Center, 204-3002 32 Ave Vernon, BC V1T 2L7, Canada*

Due to the Klein tunneling effect in graphene, it is impossible to confine or permanently localize electrons inside the graphene quantum dot. However, an electron can be transiently trapped inside the quantum dot under the effect of a constant magnetic field, which will have the so-called "quasi-bound states" characterized by a finite lifetime. In order to improve the trapping time of the electrons inside the quantum dot, we will add a mass term to the Hamiltonian, creating an energy gap. We solve the Dirac equation to determine the energy spectrum, using the continuity of the eigenspinors at the edges to study the scattering phenomenon. We find that the energy gap can increase the lifetime of the quasi bound states inside the quantum dot. In addition, we show that even in the absence of the magnetic field, the scattering efficiency can reach considerable levels when the energy gap is closed to the incident energy of the electron passing through the quantum dot. It is found that the density inside the quantum dot is enhanced, resulting in an improvement in the trapping time of the electrons.

PACS numbers: 81.05.ue; 81.07.Ta; 73.22.Pr

KEYWORDS: Graphene, circular quantum dot, magnetic field, energy gap, scattering phenomenon

I. INTRODUCTION

A two-dimensional semi-metal called graphene is distinguished by a linear band structure that is quite close to the Fermi level. It has a honeycomb lattice structure comprised entirely of carbon atoms. Researchers are very driven to enhance the conclusions established theoretically or experimentally in this context (see [1, 2]) because of the very specific electrical characteristics of graphene. The anomalous quantum Hall effect [3, 4], Klein tunneling [5], high electrical conductivity, and extremely high electron mobility [6, 7] are only a few of the extraordinary electronic characteristics of graphene. Several scientific studies have demonstrated graphene's interest in fundamental physics for more technological applications in a variety of fields (e.g., [8–10]). In-depth studies in the physics of materials like graphene are usually based on the interactions of these materials with external fields. They have shown that it can offer a perfect framework to study fundamental physics and interpret physical effects and phenomena such as Landau level quantization [11–13], Aharonov-Bohm effect [14–16]. Then graphene is one of the strongest materials tested so far, possessing remarkable conductivity qualities that serve to use graphene in technological applications such as integrated circuits, light sensing devices, and microelectronic devices [17–19].

Due to Klein's paradox, charge carriers cannot be localized in a small, constrained region of graphene by an electrostatic gate. The main objective of graphene-based electronics is to confine the particles that generate quantum dots [20–23]. Since graphene does not have a band gap, there are not any traditional quantum dots in it that can localize electrons in areas of finite dimensions. Utilizing the quantum dot for relativistic electrons, which behave like massless Dirac fermions, will be necessary for graphene's future electronic uses [2, 5]. The normal incidence issue, which is the cause of perfect transmission (Klein paradox), is resolved by using zero-dimensional circular quantum dots [24]. A variety of quantum dot applications in electronics are made possible by the possibility of confining Dirac fermions in graphene, including solar panels, lasers [25], photo-detectors [26], quantum information processing, and quantum computers [27].

The localization of graphene quantum dots is prevented by Klein tunneling when an electron strikes the dot with normal incidence [5]. The trapping of electrons in quantum dots is currently a very interesting research topic in the field of condensed matter physics. It began decades ago and continues to receive a lot of attention from both a fundamental and an application standpoint. The electron trapping problem was first studied in a one-dimensional wire in the absence of a magnetic field [20, 28, 29], and then for a quantum dot with smooth [22] and sharp [30] boundary states. The trapping potential of a relativistic electron in graphene is dependent on several factors, in particular the transverse momentum [20, 22, 31]. Regarding a quantum dot, the trapping potential is closely related to the electron's angular momentum and becomes significantly more intense as it increases. Another factor that influences the lifetime is the sharpness of the confining potential. Trapping an electron in a graphene quantum dot is thus best accomplished when the confinement potential is smooth and electronic states have a large angular momentum. It is shown that Klein tunneling is significantly reduced in the resonant regime, and the lifetime increases with increasing magnetic field [32].

A gap between the two valence and conduction bands in the graphene band structure can be made using a variety of

experimental procedures [9]. As a result of the sublattice's symmetry violation, the highest energy gap value might be 260 meV [33]. It is interesting to note that the energy gap value differs among testing techniques. By manipulating the structure of the interface between graphene and ruthenium, it has been shown that there are alternative experimental ways besides system breaking for opening gaps [34]. Furthermore, the graphene sheet's energy gap has been altered by altering the substrate, SiC is one such substrate [33]. Different band gaps are created based on depositing a graphene layer on other substrates [35, 36].

Inspired by the outcomes described above and, specifically, [32], we study the phenomenon of incident electron scattering from a gapped circular graphene quantum dot subjected to a constant magnetic field. This is an investigation into scattering efficiency Q , probability density ρ , and lifetime τ . These will allow us to show how the energy gap can affect the scattering phenomena of the present system. We first use the Dirac equation to analytically determine the solutions of the energy spectrum, and then we use the continuity at the interface to calculate the corresponding scattering efficiency outside and inside the quantum dot. We find that when the energy gap is closed to the incident energy of an electron that crosses the GQD, the efficiency can still be quite high even in the absence of a magnetic field. Also, we demonstrate that the probability density is strengthened, resulting in an improvement in the lifetime of the electrons. The main characteristics of the scattering phenomenon are analyzed in relation to the physical parameters of our present system, with the primary goal of determining the best situation to produce interesting and advantageous results.

The present paper is organized as follows. In Sec. II, we establish a theoretical model describing our system and determine the solution of the energy spectrum. After matching eigenspinors at the interface, we explicitly determine the quantities characterizing the scattering phenomenon in Sec. III. In Sec. IV, we numerically analyze our finding under various conditions of the physical parameters. The scattering efficiency Q , probability density ρ , and lifetime τ are examples. Finally, we conclude our results.

II. THEORETICAL MODEL

Let us consider a gapped circular graphene quantum dot (GQD) subjected to a constant magnetic field, which is made of two regions as depicted in Fig. 1. The current system can be described by a single valley Hamiltonian as

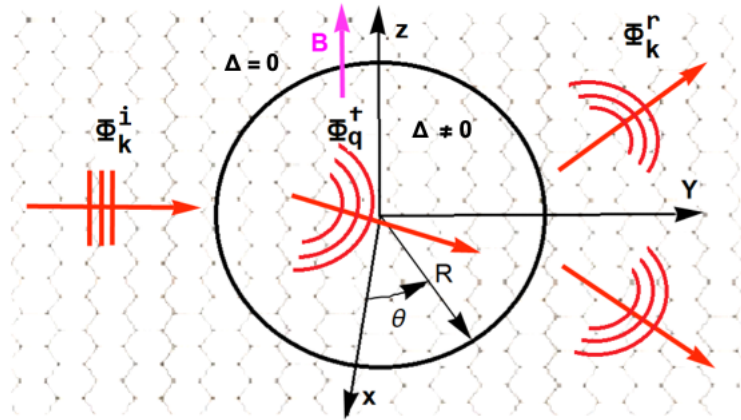


FIG. 1. (color online) A graphene quantum dot of radius R is placed in the horizontal plane xy , with the magnetic field B oriented perpendicular to the dot plane in the direction z . The incident electron is represented by a plane wave Φ_k^i with energy $E = \hbar v_F k$. When an electron approaches a quantum dot, it is either reflected (wave Φ_k^r) or transmitted (wave Φ_q^t).

follows

$$H = v_F \vec{\sigma} \cdot (\vec{p} - e\vec{A}) + \Delta \sigma_z \quad (1)$$

where $v_F = 10^6 \text{ ms}^{-1}$ is the Fermi velocity, $\vec{\sigma} = (\sigma_x, \sigma_y, \sigma_z)$ are Pauli matrices and Δ is the energy gap resulting from the mass term. It is convenient to select the vector potential $\vec{A} = \frac{B}{2}(x, y)$ in symmetric gauge. Because of the spherical symmetry, we can write the Hamiltonian in polar coordinates, knowing that

$$\sigma_r = \begin{pmatrix} 0 & e^{-i\theta} \\ e^{i\theta} & 0 \end{pmatrix}, \quad \sigma_\theta = \begin{pmatrix} 0 & -ie^{-i\theta} \\ ie^{i\theta} & 0 \end{pmatrix} \quad (2)$$

and therefore we have

$$H = \begin{pmatrix} \Delta & -i\hbar v_F e^{-i\theta} \left(\partial_r - \frac{i}{r} \partial_\theta - \frac{eBr}{2\hbar} \right) \\ -i\hbar v_F e^{-i\theta} \left(\partial_r + \frac{i}{r} \partial_\theta + \frac{eBr}{2\hbar} \right) & -\Delta \end{pmatrix}. \quad (3)$$

Given that the total angular momentum operator $J_z = -i\hbar \partial_\theta + \frac{\hbar}{2} \sigma_z$ commutes with the Hamiltonian (1), i.e., $[H, J_z] = 0$, the eigenspinors can be separated as

$$\Phi(r, \theta) = \begin{pmatrix} \Phi^A(r) e^{im\theta} \\ i\Phi^B(r) e^{i(m+1)\theta} \end{pmatrix} \quad (4)$$

where the integer values m are eigenvalue of J_z . Now using the eigenvalue equation $H\Phi(r, \theta) = E\Phi(r, \theta)$ to obtain

$$\left(\partial_r + \frac{r}{2l_B^2} - \frac{m}{r} \right) \Phi^A(r) = -\frac{E + \Delta}{\hbar v_F} \Phi^B(r) \quad (5a)$$

$$\left(\partial_r + \frac{m+1}{r} - \frac{r}{2l_B^2} \right) \Phi^B(r) = \frac{E - \Delta}{\hbar v_F} \Phi^A(r) \quad (5b)$$

For instance, by injecting (5a) into (5b), we end up with a second differential equation for $\Phi^A(r)$

$$\left(\partial_r^2 + \frac{1}{r} \partial_r + \frac{m+1}{l_B^2} - \frac{r^2}{4l_B^2} - \frac{m^2}{r^2} + q^2 \right) \Phi^A(r) = 0 \quad (6)$$

where we have set $q = \frac{\sqrt{|E^2 - \Delta^2|}}{\hbar v_F}$ and the magnetic length $l_B = \sqrt{\frac{\hbar}{eB}}$. In order to solve (6), we start by exploring the asymptotic limits that define the necessary physical behaviors depending on the value of r .

In the limit $r \rightarrow \infty$, (6) can be approximated by

$$\left(\partial_r^2 + \frac{1}{r} \partial_r - \frac{r^2}{4l_B^2} \right) \Phi^A(r) = 0 \quad (7)$$

which is the updated Bessel equation for the zero-order case, therefore having the solution

$$\Phi^A(r) = c_1 I_0 \left(\frac{r^2}{4l_B^2} \right) + c_2 K_0 \left(\frac{r^2}{4l_B^2} \right) \quad (8)$$

where $I_0(x)$ and $K_0(x)$ denote the zero order modified Bessel functions of the first and second kinds, respectively. We choose $c_1 = 0$ and $c_2 = 1$ to avoid the divergence of function $I_0(x)$ when x reaches infinity. Now using the asymptotic behavior $K_0(x) \underset{x \gg 1}{\sim} \frac{e^{-x}}{\sqrt{x}}$, to approximate $\Phi^A(r)$ as

$$\Phi^A(r) \sim 2l_B \frac{e^{-\frac{r^2}{4l_B^2}}}{r}. \quad (9)$$

In the limit $r \rightarrow 0$, (6) reduces to

$$\left(\partial_r^2 + \frac{1}{r} \partial_r - \frac{m^2}{r^2} \right) \Phi^A(r) = 0 \quad (10)$$

which has the following solution

$$\Phi^A(r) = \frac{c_3}{2} (r^m + r^{-m}) + \frac{ic_4}{2} (r^m - r^{-m}) \quad (11)$$

where c_3 and c_4 must be chosen in such a way that the solution adheres to the physical constraints. As a result, we examine the positive and negative values of m independently. Indeed, for $m \geq 0$, $\sim r^{-m}$ must vanish, which implies that $c_4 = -ic_3$ and, again by convention, we put $c_3 = 1$. For $m < 0$, $\sim r^m$ must vanish, then we replace $c_4 = ic_3$ with $c_3 = 1$. Combining all to write the asymptotic behavior of $\Phi^A(r)$ as

$$\Phi^A(r) \sim r^m, \quad m \geq 0, \quad (12a)$$

$$\Phi^A(r) \sim r^{-m}, \quad m < 0. \quad (12b)$$

Using the above analysis to write the solution of (6) as

$$\Phi^{A\pm}(r) = r^{\pm m} \frac{e^{-r^2/4l_B^2}}{r/2l_B} \Xi_q^{A\pm}(r) \quad (13)$$

knowing that the sign "+" stands for $m \geq 0$, while "-" stands for the opposite case, $m < 0$. Now, we perform the variable change $\eta = \frac{r^2}{2l_B^2}$ and use the transformation $\Xi_q^{A\pm}(\eta) = \sqrt{\eta} \chi_q^{A\pm}(\eta)$ to write (13) as

$$\Phi^{A\pm}(\eta) = l_B^{\pm m} 2^{\frac{1\pm m}{2}} \eta^{\pm m/2} e^{-\eta/2} \chi_q^{A\pm}(\eta) \quad (14)$$

which can be injected into (6) to end up with the Kummer-type differential equations

$$\eta \partial_\eta^2 \chi_q^{A+}(\eta) + (m+1-\eta) \partial_\eta \chi_q^{A+}(\eta) + \frac{l_B^2 q^2}{2} \chi_q^{A+}(\eta) = 0 \quad (15a)$$

$$\eta \partial_\eta^2 \chi_q^{A-}(\eta) + (1-m-\eta) \partial_\eta \chi_q^{A-}(\eta) + \left(m + \frac{l_B^2 q^2}{2}\right) \chi_q^{A-}(\eta) = 0 \quad (15b)$$

showing the confluent hypergeometric functions as solutions

$$\chi_q^{A+}(\eta) = {}_1F_1\left(-\frac{l_B^2 q^2}{2}, m+1, \eta\right) \quad (16a)$$

$$\chi_q^{A-}(\eta) = {}_1F_1\left(-l - \frac{l_B^2 q^2}{2}, 1-m, \eta\right). \quad (16b)$$

When we combine all of the above results, we get the following solutions to the second order differential equation (6)

$$\Phi^{A+}(r) = r^{|m|} e^{-r^2/4l_B^2} {}_1F_1\left(-\frac{l_B^2 q^2}{2}, m+1, \frac{r^2}{2l_B^2}\right) \quad (17a)$$

$$\Phi^{A-}(r) = r^{|m|} e^{-r^2/4l_B^2} {}_1F_1\left(-m - \frac{l_B^2 q^2}{2}, 1-m, \frac{r^2}{2l_B^2}\right) \quad (17b)$$

The other components of spinor (4) can be obtained by inserting (17a) and (17b) into (5a). This process yields

$$\Phi^{B+}(r) = \frac{q}{2(m+1)} r^{|m|+1} e^{-r^2/4l_B^2} {}_1F_1\left(1 - \frac{l_B^2 q^2}{2}, m+2, \frac{r^2}{2l_B^2}\right) \quad (18a)$$

$$\Phi^{B-}(r) = \frac{1}{q} r^{|m|-1} e^{-r^2/4l_B^2} \left[2m {}_1F_1\left(-m - \frac{l_B^2 q^2}{2}, 1-m, \frac{r^2}{2l_B^2}\right) + \frac{(2m + l_B^2 q^2)r^2}{2(1-m)l_B^2} {}_1F_1\left(1-m - \frac{l_B^2 q^2}{2}, 2-m, \frac{r^2}{2l_B^2}\right) \right] \quad (18b)$$

In the forthcoming analysis, we will see how the above results can be worked out to study the scattering phenomenon in terms of different quantities.

III. SCATTERING PROBLEM

In order to examine the scattering problem, we first explain how an electron scatters on a circular GQD of radius R in the presence of a constant magnetic field before identifying the key parameters that characterize the scattering problem. Consider an electron moving along the x direction with energy $E = \hbar v_F k$, where k is the corresponding wave number. As a result, the incident electron can be described by a plane wave as follows

$$\Phi_k^i(r, \theta) = \frac{1}{\sqrt{2}} e^{ikr \cos \theta} \begin{pmatrix} 1 \\ 1 \end{pmatrix} = \frac{1}{\sqrt{2}} \sum_{m=-\infty}^{\infty} i^m \begin{pmatrix} J_m(kr) e^{im\theta} \\ i J_{m+1}(kr) e^{i(m+1)\theta} \end{pmatrix} \quad (19)$$

where $J_m(z)$ is the Bessel function of first kind. The following equation demonstrates how the reflected electron wave can be divided into partial waves since it must adhere to infinite boundary requirements for the scattering mechanism being researched [37]

$$\Phi_k^r(r, \theta) = \frac{1}{\sqrt{2}} \sum_{m=-\infty}^{\infty} a_m^r i^m \begin{pmatrix} H_m(kr) e^{im\theta} \\ i H_{m+1}(kr) e^{i(m+1)\theta} \end{pmatrix} \quad (20)$$

and $H_m(x)$ is the Hankel function of first kind that is a linear combinations of J_m and Neumann Y_m , i.e., $H_m(x) = J_m(x) + iY_m(x)$. For a large value of x , its asymptotic behavior is

$$H_m(x) \underset{x \gg 1}{\sim} \sqrt{\frac{2}{\pi x}} e^{i(x - \frac{1}{2}\pi - \frac{\pi}{4})}. \quad (21)$$

The transmitted solution can be obtained from the previous analysis as

$$\Phi_q^t(r, \theta) = \sum_{m=-\infty}^{-1} a_m^{t-} \begin{pmatrix} \Phi_q^{A-}(r) e^{im\theta} \\ i\Phi_q^{B-}(r) e^{i(m+1)\theta} \end{pmatrix} + \sum_{m=0}^{\infty} a_m^{t+} \begin{pmatrix} \Phi_q^{A+}(r) e^{im\theta} \\ i\Phi_q^{B+}(r) e^{i(m+1)\theta} \end{pmatrix} \quad (22)$$

where q represents the wave number associated to the electron inside the GQD as shown in Fig. 1.

To investigate our system's scattering problem, we must first calculate the scattering coefficients a_m^r and a_m^t using the continuity of eigenspinors at the boundary condition $r = R$. This is

$$\Phi_k^i(R, \theta) + \Phi_k^r(R, \theta) = \Phi_q^t(R, \theta) \quad (23)$$

giving rise to two conditions represented by two equations of a_m^r and a_m^t

$$\frac{1}{\sqrt{2}} i^m J_m(kR) + \frac{1}{\sqrt{2}} i^m a_m^r H_m(kR) = a_m^t \Phi_q^{A\pm}(qR) \quad (24a)$$

$$\frac{1}{\sqrt{2}} i^{m+1} J_{m+1}(kR) + \frac{1}{\sqrt{2}} i^{m+1} a_m^r H_{m+1}(kR) = i a_m^t \Phi_q^{B\pm}(qR). \quad (24b)$$

Consequently, we obtain

$$a_m^{t\pm} = \frac{i\sqrt{2}e^{im\pi/2}}{\pi q R [H_m(kR) \Phi_q^{B\pm}(qR) - H_{m+1}(kR) \Phi_q^{A\pm}(qR)]} \quad (25a)$$

$$a_m^{r\pm} = \frac{-J_m(kR) \Phi_q^{B\pm}(qR) + J_{m+1}(kR) \Phi_q^{A\pm}(qR)}{H_m(kR) \Phi_q^{B\pm}(qR) - H_{m+1}(kR) \Phi_q^{A\pm}(qR)}. \quad (25b)$$

We now define the probability density function $\rho = \Phi^\dagger \Phi$ and current density $j = \Phi^\dagger \sigma \Phi$ using Hamiltonian (1), with the spinor Φ being dependent on the region where $\Phi = \Phi_t$ is inside the GQD and $\Phi = \Phi_i + \Phi_r$ is outside. As a result, the radial component of the current is given by

$$j_{\text{rad}}^r(\theta) = \Phi^\dagger \begin{pmatrix} 0 & \cos \theta - i \sin \theta \\ \cos \theta + i \sin \theta & 0 \end{pmatrix} \Phi. \quad (26)$$

Taking the asymptotic behavior (21) into account, we calculate $j_{\text{rad}}^r(\theta)$ as

$$j_{\text{rad}}^r(\theta) = \frac{4}{\pi k R} \sum_{m=-\infty}^{+\infty} |a_m^r|^2 + \frac{8}{\pi k R} \sum_{m < m'} \Re(a_m^r a_{m'}^r) \cos[(m - m')\theta]. \quad (27)$$

At this level, we are interested in the quantities related to our system to determine their basic characteristics. Indeed, in the limit $kr \rightarrow \infty$, (27) is used to calculate the effective scattering cross section σ defined by

$$\sigma = \frac{I_{\text{rad}}^r}{I^{\text{inc}}/A_u} \quad (28)$$

knowing that I_{rad}^r represents the total reflected flux through the GQD of radius R and that the incident flux per unit area represents the term I^{inc}/A_u . Our calculation shows that the total reflected flux I_{rad}^r takes the form

$$I_{\text{rad}}^r = \int_0^{2\pi} j_{\text{rad}}^r(\theta) r d\theta = \frac{8}{k} \sum_{m=-\infty}^{+\infty} |a_m|^2 \quad (29)$$

and $I^i/A_u = 1$ for the incident wave (19).

To improve our study of the scattering problem of Dirac fermions in different sizes of circular quantum dots, we analyze the scattering efficiency Q . This is defined as the ratio of the division of the scattering cross section to the geometrical cross section based on the lines shown in [38]

$$Q = \frac{\sigma}{2R} = \frac{4}{kR} \sum_{m=-\infty}^{+\infty} |a_m^r|^2. \quad (30)$$

Note that by requiring $\Delta = 0$, we recover the results found in [32]. The analytical results obtained so far will be analyzed numerically in order to study the effect of the energy gap and other parameters on the physical quantities that characterize the scattering phenomenon and also the confinement of Dirac fermions in a gapped GQD. These studies are reflected in the analysis of real space scattering and the evaluation of the lifetime corresponding to Dirac fermions inside the GQD.

IV. RESULTS AND DISCUSSIONS

We numerically examine the scattering phenomenon of electrons on a gapped GQD when it is exposed to a constant magnetic field. Our studies are based on the analysis of the magnitude in terms of scattering efficiency Q and density ρ in the region close to the quantum dot and the lifetime of the quasi-bound states. Fig. 2 represents the contour plot of Q as a function of incident energy E and magnetic field B for the radius $R = 50$ nm and different values of the energy gap Δ . Fig. 2a shows that for $\Delta = 0$, the pattern of Q is almost oscillating and consists of six bands of high values of Q , each of which corresponds to a scattering mode $m = 0, 1, 2, 3, 4, 5$, which is in agreement with the results found previously [22, 32, 39, 40]. As shown in Figs. 2(b,c,d), including the energy gap Δ reduces the resonance effect. As a result, we clearly observe that Q diminishes as long as Δ approaches the incident energy. In addition, the more the value of Δ is increased, the more the number of scattering modes is gradually decreased until it becomes only four modes when Δ approaches 40 meV, as depicted in Fig. 2d. We note that when the magnetic field corresponding to the excitation of the scattering modes decreases, the value of Δ increases.

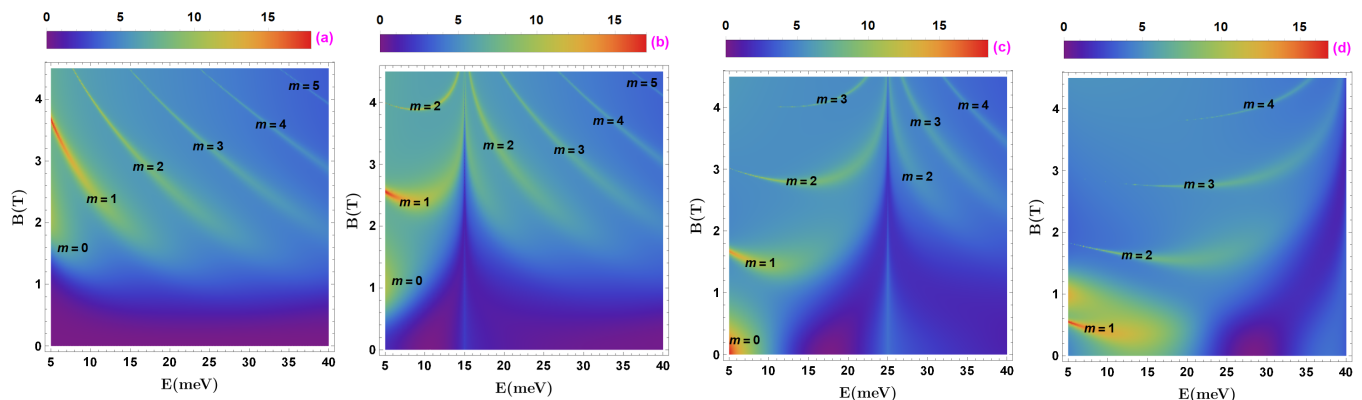


FIG. 2. (color online) The scattering efficiency Q as a function of the incident energy E and magnetic field B for $R = 50$ nm different values of Δ . (a): $\Delta = 0$ meV, (b): $\Delta = 15$ meV, (c): $\Delta = 25$ meV and (d): $\Delta = 39.5$ meV

The scattering efficiency Q is plotted as a function of the magnetic field B for various values of the energy gap Δ and incident energy E in Fig. 3. When Δ exceeds 6 meV for $E = 7$ meV and $B = 0$, Q is not null, as shown in Fig. 3a. Furthermore, we observe that Δ shifts the resonance peaks to the right. This leads to the suppression of a resonance peak at $\Delta \geq 6$ meV. In Figs. 3(b,c,d), we choose $E = 20, 25$ and 35 meV where we see that the resonance peaks are always shifted to the right due to the energy gap. Some peaks are also suppressed as Δ approaches E and Q takes specific values for $B = 0$. This tells us that Q survives and takes important values even in the absence of the magnetic field, except that one should be placed in the zone where Δ is closest to $E > 20$ meV.

We show the scattering efficiency Q as a function of the magnetic field B in Fig. 4 for $E = 20$ meV, three values of the energy gap $\Delta = 0, 14, 18$ meV and the quantum number $m = 0, \dots, 5$ meV. The first three modes, $m = -1, 0, 1$ are excited without resonance peaks in Fig. 4a for $\Delta = 0$ meV. On the other hand, for the other scattering modes $m = 2, 3, 4$, we observe resonance peaks for specific values of B . When m is increased, the width of these peaks narrows and becomes very narrow for $m = 4$. These results are in good agreement with those obtained in [32]. In Figs. 4(b,c), we see that the behavior of Q is almost similar to that found in Fig. 4a except that the positions of

the resonance peaks are shifted to the right. We also observe the suppression of the $m = 4$ scattering mode. We emphasize that in the absence of the magnetic field, the addition of Δ leads to a scattering efficiency Q no null, which becomes very important with the increase of Δ . As shown in Figs. 4(b,c), Q is solely due to the two scattering modes $m = -1, 0$.

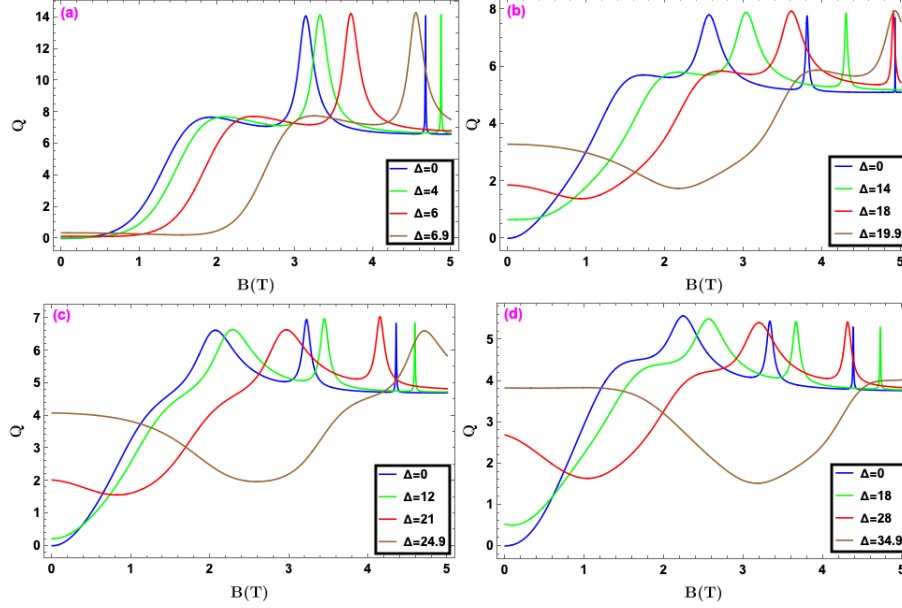


FIG. 3. (color online) The scattering efficiency Q as a function of the magnetic field B for different values of Δ and E . (a): $E = 7$ meV and $\Delta = 0, 4, 6, 6.9$ meV, (b): $E = 20$ meV and $\Delta = 0, 14, 18, 19.9$ meV, (c): $E = 25$ meV and $\Delta = 0, 12, 21, 24.9$ meV, (d): $E = 35$ meV and $\Delta = 0, 18, 28, 34.9$ meV

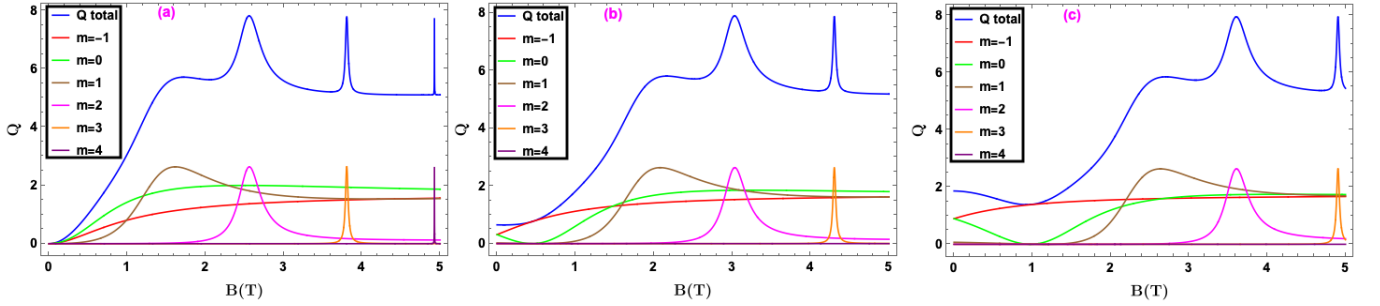


FIG. 4. (color online) The scattering efficiency Q as a function of the magnetic field B for $E = 20$ meV, $m = -1, 0, 1, 2, 3, 4$, and three values of the energy gap (a): $\Delta = 0$ meV, (b): $\Delta = 14$ meV, (c): $\Delta = 18$ meV.

The scattering efficiency Q as a function of the magnetic field B and radius R of the GQD is shown in Fig. 5 for four different values of the energy gap $\Delta = 0, 14, 18, 19.9$ meV. In Fig. 5a for $\Delta = 0$, we observe that starting from $R \approx 32$ nm, the wide bands correspond to $m = 1, 2, 3$ and narrow bands correspond to $m = 4, 5$ begin to show up. These important increases of Q are designated as "scattering resonances" and are associated with a specific scattering mode. It is clear that the interaction is very low below below $R \approx 32$ nm. Furthermore, as shown in Fig. 5a, the interaction is very weak inside the GQD, regardless of its radius, below $B \approx 0.4$ T. Now by increasing Δ in Figs. 5(b,c,d), we see that bangs appear for large values of R and grow as Δ increases. In particular, in Fig. 5d, the bangs appear for $R = 45$ nm and an energy gap $\Delta = 19.9$ meV closes to the incident one. This shows that the bangs corresponding to the scattering modes shift to larger values of R as long as Δ is increased.

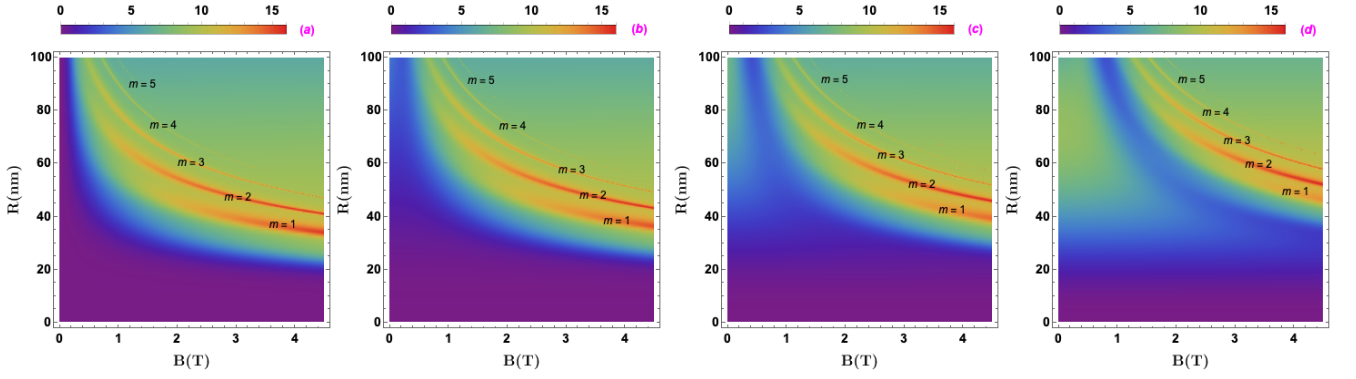


FIG. 5. (color online) The scattering efficiency Q as a function of the magnetic field B and radius R of the GQD for an incident energy value of $E = 20$ meV and four values of the energy gap (a): $\Delta = 0$ meV, (b): $\Delta = 14$ meV, (c): $\Delta = 18$ meV, (d): $\Delta = 19.9$ meV.

Fig. 6 shows Q as a function of R for $E = 20$ meV, four values of Δ and the the magnetic field (a): $B = 0.8$ T, (b): $B = 2.2$ T, (c): $B = 3.2$ T. In Fig. 6a, we observe that the most relevant resonance peaks are concentrated in the radius interval 50–100 nm. However, as B increase, we see that this interval shifts to small values of R , as shown in Figs. 6(b,c). More importantly, Q becomes significant when R is low and Δ is close to the incident energy. When R is less than 20 nm, adding an energy gap Δ increases scattering efficiency Q , but when R exceeds 20 nm, Q decreases as Δ increases.

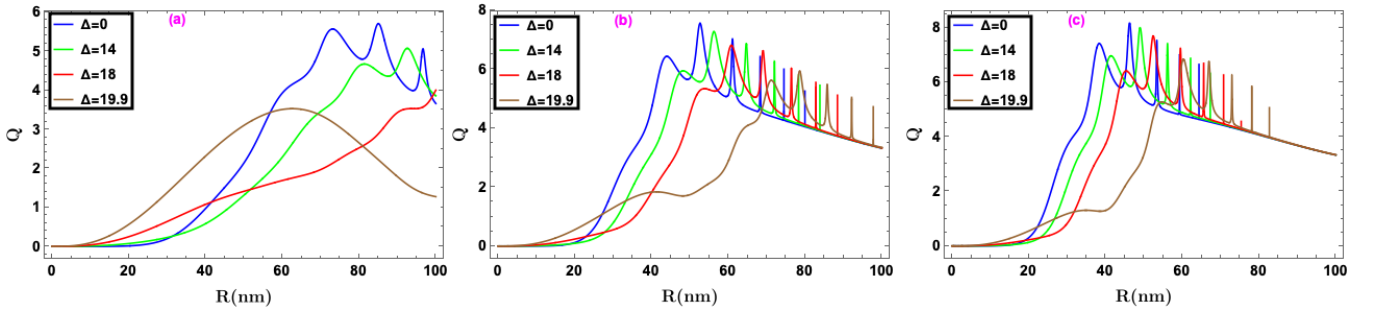


FIG. 6. (color online) The scattering efficiency Q as a function of the radius R of the GQD for three values of the magnetic field strength (a): $B = 0.8$ T, (b): $B = 2.2$ T, (c): $B = 3.2$ T, and four values of the energy gap $\Delta = 0, 14, 18, 19.9$ meV.

In Fig. 7, each column is dedicated to a scattering mode among those studied previously, and we examine the density in the field near the GQD for each mode under the effect of two values of the energy gap $\Delta = 0$ and 14 meV. The boundary of the GQD is represented by the black circle. The magnetic field values chosen correspond to the peaks of $m = 0, 1, 2, 3$ presented in Fig. 4. Line (1) starts with the results for the four scattering modes $m = 0, 1, 2, 3$ at zero energy gap. In Fig. 7a where $B = 0.4$ T, we see that the large values of the density are distributed in the outer part of the GQD, i.e., the electron wave is diffracted on the GQD boundary, as can be observed in Fig. 4a where only the $m = -1, 0$ modes are non-resonantly excited with a very low value of the scattering efficiency. Thus, in this case, we do not expect electron trapping effects inside the GQD. The mode $m = 1$ is resonantly excited with a broad peak in Fig. 7c for $B = 1.62$ T. With the presence of the diffraction bands, we also observe that the majority of the density is localized outside the GQD, but now the near field density values are slightly larger. The mode $m = 2$ is excited with a narrower resonance peak in Fig. 7e for $B = 2.56$ T than in the previous case. In this case, the majority of the density is concentrated inside the GQD with a high scattering efficiency. As a result, the small resonance peak of the mode $m = 2$ makes it more likely that the electron will be trapped inside the GQD. The resonance of the mode $m = 3$ is very clear in Fig. 7g for $B = 3.8$ T, with a narrower peak than for $m = 2$. We see the density concentration inside the GQD with a higher scattering efficiency and the suppression of diffraction bands. Therefore, the electron trapping effect inside the quantum dot is notable. From the aforementioned, we infer that the trapping effect increases with the resonance peak's narrowness. In line (2), we represent the results obtained at an energy gap $\Delta = 14$ meV for the four scattering modes $m = 0, 1, 2, 3$ with (b): ($m = 0, B = 0.8$ T) and (d): ($m = 1, B = 2.1$ T). It is clearly seen that the density inside and at the GQD boundary is improved compared to those seen before, with the presence of diffraction bands around the GQD. Comparing (f): ($m = 2, B = 3.03$ T) and (h): ($m = 3, B = 4.3$ T) with (e) and

(g), we see that the density is more concentrated inside the GQD and has created a clearer cloud around the core of the GQD. Therefore, when an energy gap is added, the impact of electron trapping inside the GQD is improved.

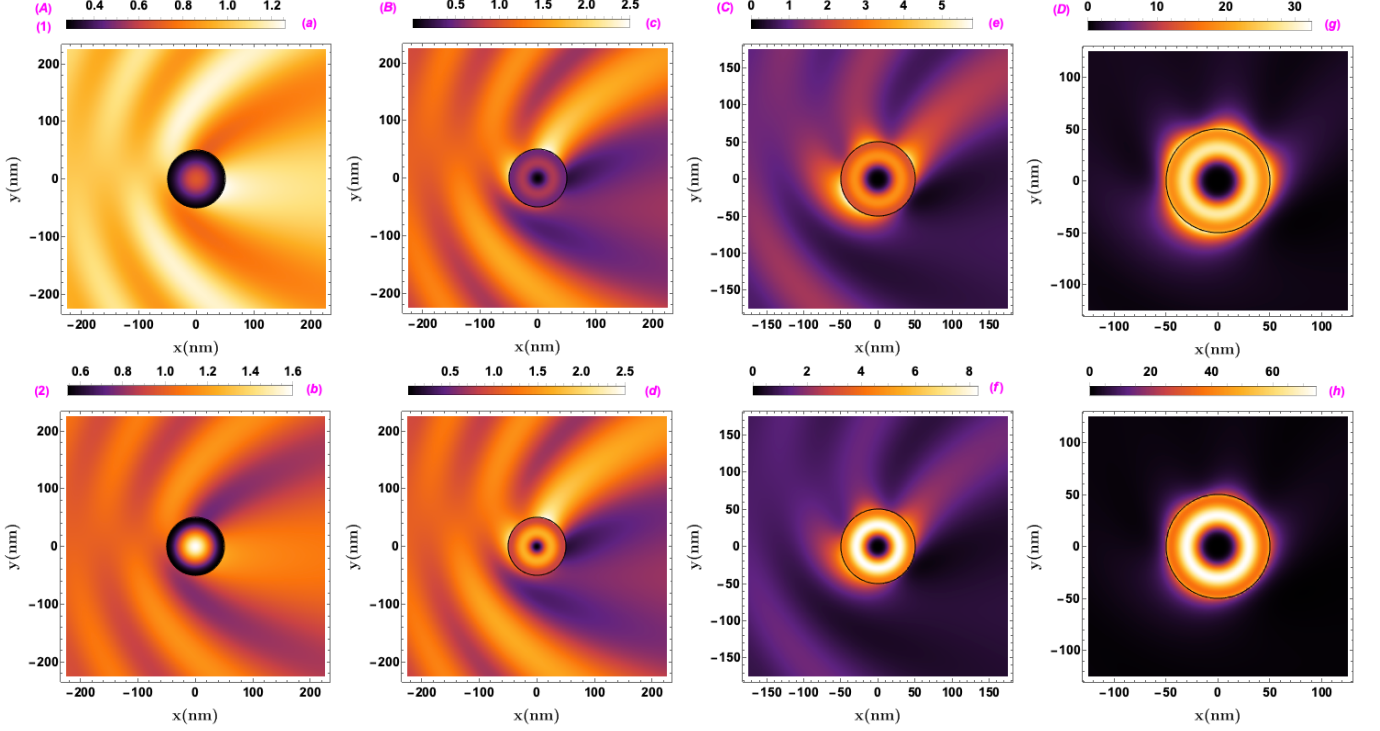


FIG. 7. (color online) A density representation for a real space examination of electron scattering on a magnetically driven GQD. Each graph column is devoted to a given value of the quantum number (A): $m = 0$, (B): $m = 1$, (C): $m = 2$, and (D): $m = 3$. Each graph line represents a specific value of the energy gap (1): $\Delta = 0$ meV and (2): $\Delta = 14$ meV. Each panel corresponds to a given value of magnetic field (a): $B = 0.4$ T, (b): $B = 0.8$ T, (c): $B = 1.62$ T, (d): $B = 2.1$ T, (e): $B = 2.56$ T, (f): $B = 3.03$ T, (g): $B = 3.8$ T, (h): $B = 4.3$ T. A black circle indicates the geographic extent of the GQD.

We now perform another analysis in terms of density in real space to evaluate the trapping time (the lifetime of the quasi-bound states). The analysis of the scattering resonances must be performed in terms of the complex incident electronic energy $E = E_r - iE_i$, where E_r represents the resonance energy and E_i gives the lifetime of the quasi-bound states τ , with $\tau = \hbar/E_i$. We have previously indicated that the whole scattering process can be decomposed into several scattering sub-processes. We will now concentrate on the two scattering modes $m = 0, 3$ to see how the energy gap Δ affects the lifetime τ of the quasi-bound states. We use continuity to find the complex energy of the incident electron by matching the transmitted wave function with the reflected wave function on the boundary $r = R$ [39]. Since the incident energy of the incoming electron is not affected by the magnetic field, we treat the following transcendental equation for q and k

$$\frac{\Phi_q^{A\pm}(qR)}{\Phi_q^{B\pm}(qR)} = \frac{H_m(kR)}{H_{m+1}(kR)}. \quad (31)$$

The lifetime τ as a function of the magnetic field B is shown in Fig. 8 for the two scattering modes $m = 0, 3$ and four values of the energy gap $\Delta = 0, 14, 18, 19.9$ meV. The first thing we notice is that τ increases as B increases, which agrees with what we previously discovered by examining the scattering efficiency Q . In Fig. 8a, τ becomes visible from $B = 1.8$ T and increases more clearly from $B \approx 3.35$ T for Δ non-null. In Fig. 8b, we see that for a given Δ , τ tends to increase from small values of B when compared to the case of $\Delta = 0$ for higher magnetic fields. We conclude that when Δ is non-null, τ improves even further.

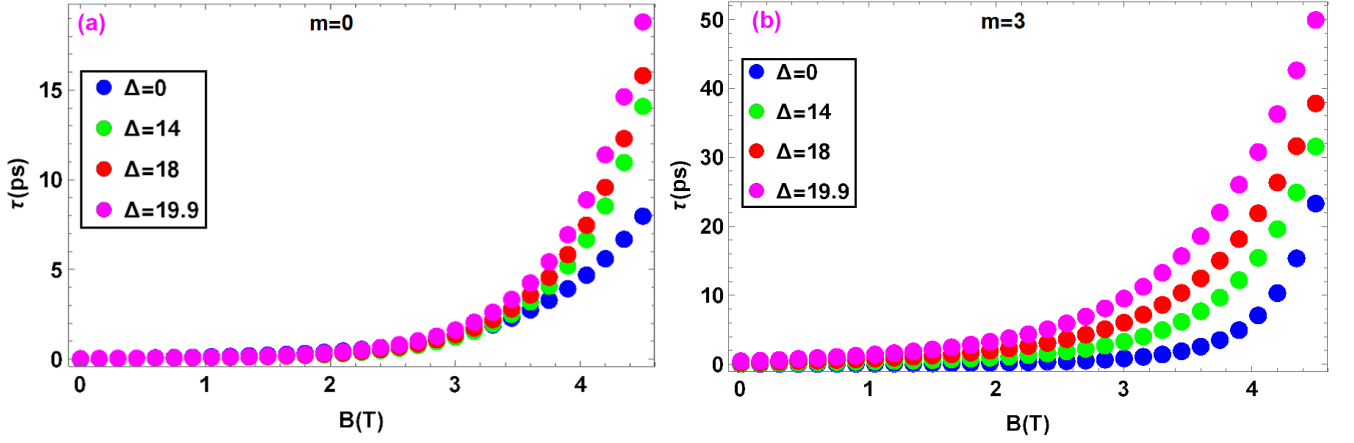


FIG. 8. (color online) The lifetime τ as a function of magnetic field B for four values of the energy gap $\Delta = 0, 14, 18, 19.9$ meV and two scattering modes (a): $m = 0$, (b): $m = 3$.

V. CONCLUSION

The theoretical analysis of the electron scattering mechanism on a magnetically driven graphene quantum dot (GQD) in the presence of a mass term generating an energy gap in the spectrum has been further investigated. In this regard, we first established a theoretical model for the interaction of Dirac fermions with a constant magnetic field in a circular GQD and identified the crucial variables. To deal with the problem correctly, we first solved the corresponding Dirac equation and analytically determined the energy spectrum. Using the continuity of the eigenspinors, we calculated different quantities characterizing the scattering phenomenon. In particular, the efficiency Q is found to be dependent on the magnetic field, angular momentum, radius of the GQD, incident energy, and energy gap.

We also presented numerically the obtained results to provide a general interpretation of the scattering phenomenon and to show how an electron at normal incidence can be trapped in a GQD for a certain period of time, with the main objective being to improve this trapping time. We discovered that even in the absence of a magnetic field, scattering efficiency can reach significant values when the energy gap is close to the incident energy of the electron crossing the GQD. For a non-null magnetic field, we showed that the resonance peaks with a higher scattering efficiency are those corresponding to the smallest values of radius of the GQD.

By analyzing the probability density, we showed that the diffraction phenomenon is dominant in the domain where the scattering is non-resonant, with a weak localization of the density in the GQD without an energy gap. However, when an energy gap is added, it is found that the density inside the GQD is enhanced. On the other hand, in the domain where the scattering is resonant, we noticed the damping of the diffraction with a very important localization of the density inside and at the boundary of the GQD, as well as with noticeable trapping effects. The important result in our paper is to improve the possibility of trapping electrons in the GQD under the influence of a mass term, creating an energy gap in the energy spectrum.

ACKNOWLEDGMENTS

We warmly thank Professor Adrian Pena for his valuable support.

-
- [1] K. S. Novoselov, A. K. Geim, S. V. Morozov, D.-e. Jiang, Y. Zhang, S. V. Dubonos, I. V. Grigorieva, and A. A. Firsov, Electric field effect in atomically thin carbon films, *science* **306**, 666 (2004).
 - [2] K. S. Novoselov, A. K. Geim, S. V. Morozov, D. Jiang, M. I. Katsnelson, I. Grigorieva, S. Dubonos, and a. Firsov, Two-dimensional gas of massless dirac fermions in graphene, *nature* **438**, 197 (2005).
 - [3] V. Gusynin and S. Sharapov, Unconventional integer quantum hall effect in graphene, *Physical review letters* **95**, 146801 (2005).

- [4] B. Ostahie, M. Niță, and A. Aldea, Electrical manipulation of edge states in graphene and the effect on quantum hall transport, *Physical Review B* **91**, 155409 (2015).
- [5] M. Katsnelson, K. Novoselov, and A. Geim, Chiral tunnelling and the klein paradox in graphene, *Nature physics* **2**, 620 (2006).
- [6] A. K. Geim and K. S. Novoselov, The rise of graphene, *Nature materials* **6**, 183 (2007).
- [7] A. K. Geim, Graphene: status and prospects, *science* **324**, 1530 (2009).
- [8] A. C. Neto, F. Guinea, N. M. Peres, K. S. Novoselov, and A. K. Geim, The electronic properties of graphene, *Reviews of modern physics* **81**, 109 (2009).
- [9] D. Abergel, V. Apalkov, J. Berashevich, K. Ziegler, and T. Chakraborty, Properties of graphene: a theoretical perspective, *Advances in Physics* **59**, 261 (2010).
- [10] V. N. Kotov, B. Uchoa, V. M. Pereira, F. Guinea, and A. C. Neto, Electron-electron interactions in graphene: Current status and perspectives, *Reviews of modern physics* **84**, 1067 (2012).
- [11] F. Guinea, A. C. Neto, and N. Peres, Electronic states and landau levels in graphene stacks, *Physical Review B* **73**, 245426 (2006).
- [12] V. Lukose, R. Shankar, and G. Baskaran, Novel electric field effects on landau levels in graphene, *Physical review letters* **98**, 116802 (2007).
- [13] L.-J. Yin, S.-Y. Li, J.-B. Qiao, J.-C. Nie, and L. He, Landau quantization in graphene monolayer, bernal bilayer, and bernal trilayer on graphite surface, *Physical Review B* **91**, 115405 (2015).
- [14] P. Recher, B. Trauzettel, A. Rycerz, Y. M. Blanter, C. Beenakker, and A. Morpurgo, Aharonov-bohm effect and broken valley degeneracy in graphene rings, *Physical Review B* **76**, 235404 (2007).
- [15] J. Heini, M. Schneider, and P. W. Brouwer, Interplay of aharonov-bohm and berry phases in gate-defined graphene quantum dots, *Physical Review B* **87**, 245426 (2013).
- [16] D. Żebrowski, A. Mreńca-Kolasińska, and B. Szafran, Aharonov-bohm conductance oscillations and current equilibration in local n- p junctions in graphene, *Physical Review B* **98**, 155420 (2018).
- [17] G. Konstantatos, M. Badioli, L. Gaudreau, J. Osmond, M. Bernechea, F. De Arquer, F. Gatti, and F. H. Koppens, Hybrid graphene–quantum dot phototransistors with ultrahigh gain, *Nature nanotechnology* **7**, 363 (2012).
- [18] K. Dani, J. Lee, R. Sharma, A. Mohite, C. Galande, P. Ajayan, A. Dattelbaum, H. Htoon, A. Taylor, and R. Prasankumar, Intraband conductivity response in graphene observed using ultrafast infrared-pump visible-probe spectroscopy, *Physical Review B* **86**, 125403 (2012).
- [19] E. Gruber, R. A. Wilhelm, R. Pétuya, V. Smejkal, R. Kozubek, A. Hierzenberger, B. C. Bayer, I. Aldazabal, A. K. Kazansky, F. Libisch, *et al.*, Ultrafast electronic response of graphene to a strong and localized electric field, *Nature communications* **7**, 1 (2016).
- [20] P. Silvestrov and K. Efetov, Quantum dots in graphene, *Physical Review Letters* **98**, 016802 (2007).
- [21] A. De Martino, L. Dell’Anna, and R. Egger, Magnetic confinement of massless dirac fermions in graphene, *Physical review letters* **98**, 066802 (2007).
- [22] H.-Y. Chen, V. Apalkov, and T. Chakraborty, Fock-darwin states of dirac electrons in graphene-based artificial atoms, *Physical review letters* **98**, 186803 (2007).
- [23] T. G. Pedersen, C. Flindt, J. Pedersen, N. A. Mortensen, A.-P. Jauho, and K. Pedersen, Graphene antidot lattices: designed defects and spin qubits, *Physical Review Letters* **100**, 136804 (2008).
- [24] T. Chakraborty, *Comments condens. matter phys.* **16**, 35 (1992); pa maksym and t. chakraborty, *Phys. Rev. Lett* **65**, 108 (1990).
- [25] S. Fafard, K. Hinzer, S. Raymond, M. Dion, J. McCaffrey, Y. Feng, and S. Charbonneau, Red-emitting semiconductor quantum dot lasers, *Science* **274**, 1350 (1996).
- [26] H. Liu, M. Gao, J. McCaffrey, Z. Wasilewski, and S. Fafard, Quantum dot infrared photodetectors, *Applied Physics Letters* **78**, 79 (2001).
- [27] D. Loss and D. P. DiVincenzo, Quantum computation with quantum dots, *Physical Review A* **57**, 120 (1998).
- [28] B. Trauzettel, D. V. Bulaev, D. Loss, and G. Burkard, Spin qubits in graphene quantum dots, *Nature Physics* **3**, 192 (2007).
- [29] L. Brey and H. Fertig, Electronic states of graphene nanoribbons studied with the dirac equation, *Physical Review B* **73**, 235411 (2006).
- [30] A. Matulis and F. M. Peeters, Quasibound states of quantum dots in single and bilayer graphene, *Physical Review B* **77**, 115423 (2008).
- [31] V. V. Cheianov and V. I. Fal’ko, Selective transmission of dirac electrons and ballistic magnetoresistance of n- p junctions in graphene, *Physical review b* **74**, 041403 (2006).
- [32] A. Pena, Electron trapping in magnetic driven graphene quantum dots, *Physica E: Low-dimensional Systems and Nanostructures* **141**, 115245 (2022).
- [33] S. Y. Zhou, G.-H. Gweon, A. Fedorov, d. First, PN, W. De Heer, D.-H. Lee, F. Guinea, A. Castro Neto, and A. Lanzara, Substrate-induced bandgap opening in epitaxial graphene, *Nature materials* **6**, 770 (2007).
- [34] C. Enderlein, Y. Kim, A. Bostwick, E. Rotenberg, and K. Horn, The formation of an energy gap in graphene on ruthenium by controlling the interface, *New Journal of Physics* **12**, 033014 (2010).
- [35] S. Rusponi, M. Papagno, P. Moras, S. Vlaic, M. Etzkorn, P. Sheverdyaeva, D. Pacilé, H. Brune, and C. Carbone, Highly anisotropic dirac cones in epitaxial graphene modulated by an island superlattice, *Physical review letters* **105**, 246803 (2010).

- [36] H. Kim, N. Leconte, B. L. Chittari, K. Watanabe, T. Taniguchi, A. H. MacDonald, J. Jung, and S. Jung, Accurate gap determination in monolayer and bilayer graphene/h-bn moiré superlattices, *Nano letters* **18**, 7732 (2018).
- [37] J. Cserti, A. Pályi, and C. Péterfalvi, Caustics due to a negative refractive index in circular graphene p- n junctions, *Physical review letters* **99**, 246801 (2007).
- [38] C. Schulz, R. Heinisch, and H. Fehske, Electron flow in circular graphene quantum dots, *arXiv preprint arXiv:1412.2539* (2014).
- [39] P. Hewageegana and V. Apalkov, Electron localization in graphene quantum dots, *Physical Review B* **77**, 245426 (2008).
- [40] Z.-Q. Fu, K.-K. Bai, Y.-N. Ren, J.-J. Zhou, and L. He, Coulomb interaction in quasibound states of graphene quantum dots, *Physical Review B* **101**, 235310 (2020).